



CrossMark  
 click for updates

Cite this: *RSC Adv.*, 2017, 7, 12561

# Synthesis and characterization of a tin(IV) antimonophosphate nano-composite membrane incorporating 1-dodecyl-3-methylimidazolium bromide ionic liquid

Sandeep Kaushal,<sup>a</sup> Gurbir Singh,<sup>b</sup> Pritpal Singh<sup>\*a</sup> and Tejwant Singh Kang<sup>\*b</sup>

The fabrication of polyvinyl chloride (PVC) based cation exchange nano-composite membranes by the solution casting technique using tetrahydrofuran as solvent and tin(IV) antimonophosphate as cation exchanger has been achieved. An ionic liquid (IL), 1-dodecyl-3-methylimidazolium bromide, [C<sub>12</sub>mim][Br], was used as a filler additive, which has been found to affect the properties of the composite membrane. From X-ray diffraction (XRD), it has been observed that membrane with a mass ratio of tin(IV) antimonophosphate (exchanger) : PVC (binder) : IL of 1 : 1 : 0.3 (M-3) has higher crystallinity than other membranes having a composition of 1 : 1 : 0.1 (M-1), 1 : 1 : 0.2 (M-2), 1 : 1 : 0.4 (M-4), and 1 : 1 : 0.5 (M-5). The nano-composite membranes are composed of interconnecting networks of near spherical to hexagonal nano-particles of 30–40 nm with nanophase separations at the surface, specifically in the case of M-3. An increase in the concentration of the IL in the casting solution led to a decrease in water content of the membrane and ion exchange capacity (IEC). The membrane potential, transport number, permselectivity and fixed charge density have been found to be higher for monovalent metal ions as compared to that of bivalent metal ions. The membrane M-3 has shown the best results among the investigated membranes.

Received 25th November 2016  
 Accepted 15th February 2017

DOI: 10.1039/c6ra27318a

rsc.li/rsc-advances

## 1. Introduction

Ion exchange membranes (IEMs) have been utilized as active separators in numerous electrically driven processes like demineralization of sugarcane juice, manufacturing of basic chemical products and environmental remediation such as treatment of industrial and biological effluents.<sup>1–13</sup> Due to low energy requirements, these processes are economically viable and advances in membrane technology can make these better than traditional processes, which are energy intensive, environmentally undesirable and costly.<sup>14–16</sup> Various researchers have used plasticized polymeric substances, generally polyvinylchloride (PVC),<sup>17,18</sup> polycarbonate (PC)<sup>2,3</sup> and cellulose triacetate (CTA),<sup>19,20</sup> as a copolymer for the fabrication of ion exchange membranes (IEMs). In the current scenario, ionic liquids (ILs), a new kind of materials which are solely composed of ions and have melting points at least below 100 °C, have attracted the attention of researchers around the globe. The basis of such huge interest in ILs lies in some unique physico-chemical properties such as high ionic conductivity, non-

volatility, high thermal stability, varying polarity, non-flammability and broad electrochemical window *etc.*<sup>21–23</sup> Owing to these properties, ILs have found a place in various applications such as in catalysis,<sup>24,25</sup> synthesis,<sup>25</sup> extraction and separation,<sup>26,27</sup> organic synthesis, and electrolytes in super capacitors,<sup>28</sup> and for dissolution and stabilization of a variety of biomolecules.<sup>29–31</sup> Besides this, ILs have been successfully tested as electrolytes in various electrochemical devices like batteries, solar cells, fuel cells, supercapacitors *etc.*,<sup>32–35</sup> due to their better electrochemical stability, high conductivity and good solvation properties. Moreover, ILs have been used for fabrication of proton conducting composite membranes because of their unique physicochemical properties such as high polarity, ionic conductivity, high heat capacity as well as chemical and thermal stabilities.<sup>36,37</sup> Further, a variety of anion exchange membranes have been reported utilizing the ILs for better performance and stability.<sup>38–41</sup> Guo *et al.*, have reported anion exchange membranes based on the copolymers of 1-allyl-3-methylimidazolium chloride (AmimCl) either with methyl methacrylate (MMA) or butyl methacrylate (BMA) and highlighted the thermal and chemical stability of the membrane including its suitability for alkaline fuel cell.<sup>38</sup> Wang *et al.*, reported anion exchange membrane prepared *via in situ* assembly of *N*-dodecyl-imidazole and 1,4-dibromobutane to construct the bi-imidazolium functionalized cationic liquid monomer, butanediyl-1,4-bis(*N*-dodecylimidazole bromide) into

<sup>a</sup>Department of Chemistry, Sri Guru Granth Sahib World University, Fatehgarh Sahib, Punjab, India. E-mail: dhillonps2003@gmail.com

<sup>b</sup>Department of Chemistry, UGC-centre for Advance Studies – II, Guru Nanak Dev University, Amritsar, 143005, India. E-mail: tejwantsinghkang@gmail.com



the isopropanol dispersions of quaternized chitosan, followed by anion exchange with  $\text{OH}^-$ . The prepared membrane has been shown to exhibit high anionic conductivity up to a temperature of  $80\text{ }^\circ\text{C}$  along with long term stability in aqueous solutions of  $\text{KOH}$ .<sup>39</sup> In all these reports, the ILs have been covalently bound with the polymers. It is expected that the weaker interactions between the polymer and constituent ions of IL would affect the morphology, internal structure and performance, especially due to mobility of the ions of IL in the membrane. Similarly, the reports pertaining to preparation of cation exchange membranes are very limited. A heterogeneous cation exchange membrane based on PVC using IL as a plasticizer has been reported, which has shown high transport number.<sup>40</sup>

In the present work, nano-composite heterogeneous cation exchange membranes based on inorganic ion exchanger tin(IV) antimonophosphate and 1-dodecyl-3-methylimidazolium bromide,  $[\text{C}_{12}\text{mim}][\text{Br}]$ , have been fabricated by solution casting technique and phase inversion method.<sup>41</sup> The influence of varying ratio of IL on physico-chemical, morphological and electrochemical properties of the fabricated membranes has been investigated. Polyvinylchloride (PVC) was used as a film-forming binder and tetrahydrofuran (THF) as solvent. The novelty of the present work lies in the fact that there exist no report on heterogeneous cation exchange membranes based on tin(IV) antimonophosphate and a long chain IL, 1-dodecyl-3-methylimidazolium bromide,  $[\text{C}_{12}\text{mim}][\text{Br}]$ , which has been found to exert a great influence on the behavior of synthesized membrane. The use of long chain IL having weaker interactions with the ion exchanger is expected to improve the performance of membrane without leaching out.

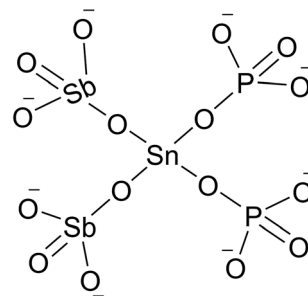
## 2. Experimental

### 2.1. Materials & methods

1-Methylimidazole (>98%), 1-bromododecane (>98%), tin(IV) chloride (98%), potassium pyroantimonate (AR Sigma Aldrich), and polyvinylchloride (PVC) (AR Sigma Aldrich) have been purchased from Sigma and used without further purification. Phosphoric acid (88–93%) was purchased from Vetec. THF, diethyl ether and acetone (AR Grade) were purchased from Spectrochem, India. The IL, 1-dodecyl-3-methylimidazolium bromide,  $[\text{C}_{12}\text{mim}][\text{Br}]$ , has been synthesized by using a well established protocol and characterized by  $^1\text{H}$  NMR technique.<sup>42</sup> The possible structure of prepared Sn(IV) SbP is shown in Scheme 1.

### 2.2. Synthesis of tin(IV) antimonophosphate cation exchanger

Sol-gel method was employed for the synthesis of tin(IV) antimonophosphate ion-exchanger. 0.1 M tin(IV) chloride solution was added to a continuously stirred mixture of 0.1 M potassium pyroantimonate and 0.1 M phosphoric acid solutions at  $60\text{ }^\circ\text{C}$  for 6 h, in the volume ratio 2 : 1 : 1. The gel formed was permitted to stand overnight. The gel was repeatedly washed with distilled water to remove chloride ions. The gel was then filtered and dried in an air oven at  $40\text{ }^\circ\text{C}$ .



Scheme 1 Showing the possible structure of Sn(IV) SbP ion exchanger.

### 2.3. Fabrication of Sn(IV) antimonophosphate cation exchanger-IL nano-composite membrane

The heterogeneous cation exchange membranes were prepared by solution casting technique. Dry tin antimonophosphate was crushed to a fine powder to facilitate the membrane preparation. Polyvinylchloride (PVC) binder was dissolved in THF (THF : PVC = 20 : 1, v/w) in a flat bottom flask by stirring for 6 h. A definite quantity of powdered exchanger (exchanger : PVC = 1 : 1, w/w) and IL (0.0, 10, 20, 30, 40%) were added in polymeric solution. The composition of casting solution is given in Table 1. Five different mass ratios of tin(IV) antimonophosphate (exchanger) : PVC (binder) and IL as 1 : 1 : 0.1; 1 : 1 : 0.2; 1 : 1 : 0.3; 1 : 1 : 0.4 and 1 : 1 : 0.5 have been used to prepared five membranes differing in composition and abbreviated as M-1, M-2, M-3, M-4 and M-5, respectively. The solution was sonicated for one hour to ensure uniform dispersion of particles,<sup>43</sup> followed by magnetic stirring for 30 minutes. The mixture was then poured into glass ring fitted on a clean and dry glass plate. The solvent was allowed to evaporate overnight at room temperature. The membranes obtained were immersed in distilled water overnight and then in 0.5 M NaCl solution for 48 h.

### 2.4. Characterization of membrane

The physico-chemical characterization of tin(IV) antimonophosphate-IL (SnSbP-IL) nano-composite membranes was achieved by various analytical techniques. The crystalline or amorphous nature of the prepared membrane was tested by using X-ray diffractometer (PAN analytical, system no. DY 3190) in the  $2\theta$  range  $10\text{--}80^\circ$ . The surface morphology of the membrane was monitored by Zeiss Ultra 55-Limited edition scanning electron microscope (SEM). Transmission electron microscopy (TEM) has been performed employing JEM-2100 transmission electron microscope at a working voltage of 200 kV without staining the sample. For SEM and TEM measurements, a drop of the suspension of crushed membrane in ethanol was placed on thoroughly cleaned glass surface and carbon coated copper grid (300 mesh), respectively. The samples were dried at  $35\text{ }^\circ\text{C}$  for 24 hours prior to measurement. The water content, membrane porosity, thickness and the ion exchange capacity of the membranes was measured using standard set of procedures as described below.

The ion exchange capacity was determined by the titration method. The membrane was placed in 1 M HCl solution for 24



Table 1 Composition and effect of IL loading on physicochemical properties of the membranes

Membrane number	Composition (exchanger : binder (PVC) : IL)	Thickness (mm)	Water content (%)	Porosity	Na <sup>+</sup> ion IEC (meq g <sup>-1</sup> )
M-1	1 : 1 : 0.0	0.49	18.27	4.18 × 10 <sup>-4</sup>	1.15
M-2	1 : 1 : 0.1	0.53	16.31	5.30 × 10 <sup>-4</sup>	1.02
M-3	1 : 1 : 0.2	0.51	15.41	5.90 × 10 <sup>-4</sup>	0.91
M-4	1 : 1 : 0.3	0.52	12.01	6.20 × 10 <sup>-4</sup>	0.87
M-5	1 : 1 : 0.4	0.51	10.31	5.70 × 10 <sup>-4</sup>	0.72

hours to convert its exchangeable groups to H<sup>+</sup> form. The membrane was then washed with distilled water to remove the excess acid followed by keeping the membrane in 0.1 M NaNO<sub>3</sub> solution for 8 hours. This solution was titrated against 0.01 M NaOH solution using phenolphthalein indicator and IEC was obtained using the following equation.<sup>44</sup>

$$\text{IEC} = \frac{N \times V}{W} \text{meq g}^{-1} \quad (1)$$

where  $N$  and  $V$  are normality and volume in ml of NaOH, respectively, and  $W$  is mass in gram of the SnSbP-IL membrane.

Water content of the membranes was measured as the mass difference between the dried and swollen membranes. The wet membrane was weighed and then dried in oven until a constant weight was obtained. The water content was calculated by the following equation:<sup>45</sup>

$$\text{Water content \%} = \frac{W_{\text{wet}} - W_{\text{dry}}}{W_{\text{dry}}} \times 100 \quad (2)$$

where  $W_{\text{wet}}$  and  $W_{\text{dry}}$  are the mass (g) of wet and dry membrane, respectively.

Porosity is regarded as the volume of water incorporated in the cavities per unit membrane volume, and is calculated by the following relation:<sup>46</sup>

$$\varepsilon = \frac{m_w - m_d}{AL\rho_w} \quad (3)$$

where  $m_w$  and  $m_d$  are the mass (g) of wet and dry membrane, respectively,  $L$  is the thickness of the membrane,  $A$  is the area of the membrane, and  $\rho_w$  is the density of water.

The thickness of the membrane was measured by a vernier caliper. The difference between the average thickness of the membrane equilibrated with 1 M NaCl for 24 h and the dry membrane is a measure of swelling. The electrochemical characterization of the membrane was performed using (digital potentiometer, Systronic 318) and different parameters of interest such as membrane potential, transport number, permselectivity and fixed charge density have been deduced. The transport number ( $\bar{t}_+$ ) was calculated from the membrane potential by the following equation:

$$E_m = 2.303 \frac{RT}{nF} (2\bar{t}_+ - 1) \log \frac{C_2}{C_1} \quad (4)$$

where  $R$  is gas constant,  $F$  is Faraday constant,  $T$  is absolute temperature,  $C_1$  &  $C_2$  are the concentrations of electrolyte solution in the test cell. The ionic permselectivity of membrane

has been calculated on the basis of migration of counter ions through cation exchange membrane *i.e.* from the transport numbers<sup>47-51</sup> using the following equation:

$$P_s = (\bar{t}_+ - t_+) / (1 - t_+) \quad (5)$$

where  $\bar{t}_+$  refers to the value of transport number in the membrane phase and  $t_+$  is the transport number of counter ions in solution.<sup>52</sup>

### 3. Results and discussion

#### 3.1. X-ray diffraction studies

The nature of the prepared membranes as amorphous or crystalline has been investigated using X-ray diffraction (XRD) measurements. Fig. 1 shows the XRD profiles of the prepared membranes.

As can be seen from Fig. 1, the prepared membranes with lower content of IL (M-1 and M-2) as well as relatively higher content of IL (M-5) are no doubt amorphous in nature. However, the membranes at intermediate concentration range of IL (M-3 and M-4) seem to be crystalline in nature. In general, with increase in content of IL up to M-3, the crystallinity of the membrane increases followed by a decrease at higher content of IL (M-5). It is expected that the increased content of IL leads to enhanced interactions between hydrophobic backbone of PVC and long hydrophobic alkyl chain of IL, which results into

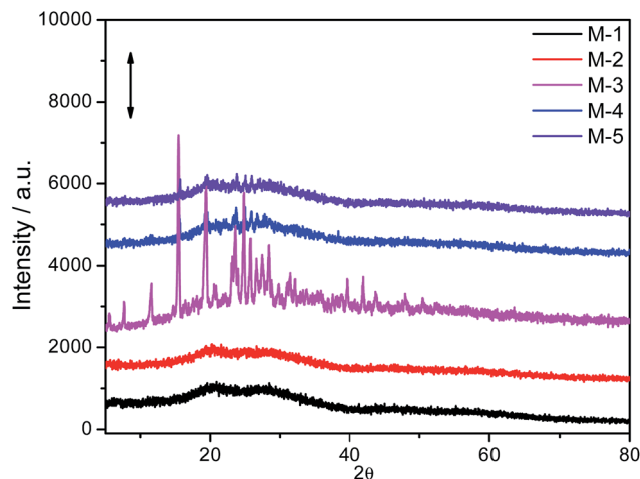


Fig. 1 XRD profiles of the fabricated nano-composite membranes.



conformational modification in a way that there is increase in packing density in an ordered manner. This leads to appearance of crystallinity in the membranes. The micro-phase separation (discussed later) in the membrane, especially in case of M-3 and M-4, could also lead to appearance of crystallinity. On the other hand, at very high content of IL (M-5), the IL-IL interactions overcome the IL-PVC interactions, thereby again resulting in amorphous nature of the membrane. The crystalline nature of the membrane has been found to affect various characteristic properties of the membrane, which is discussed later.

### 3.2. Surface morphology of composite membranes

The surface morphology of the prepared membranes has been monitored by scanning electron microscopy (SEM). Fig. 2(A-E)

shows the SEM images of the prepared membranes. All the nano-composite membranes seems to be composed of small globular particles (inset of Fig. 2A) having size  $\approx 20-50$  nm, associated with each other. It has been observed that while going from M-1 to M-4, the porous nature of the composite membranes increases as evidenced by enhanced cracks at the surface of membranes by SEM measurements. It is natural to assume that the inefficient packing of small globular particles leads to porosity in the membranes. With further increase in content of IL (M-5), again the porosity seems to decrease. Such variation in porosity with variation of IL content is expected to have drastic effect on other physico-chemical properties of the prepared membranes. Further, a careful examination of the nano-composite membranes reveals the presence of additional nano-particles, which are spherical to triangular in shape, on

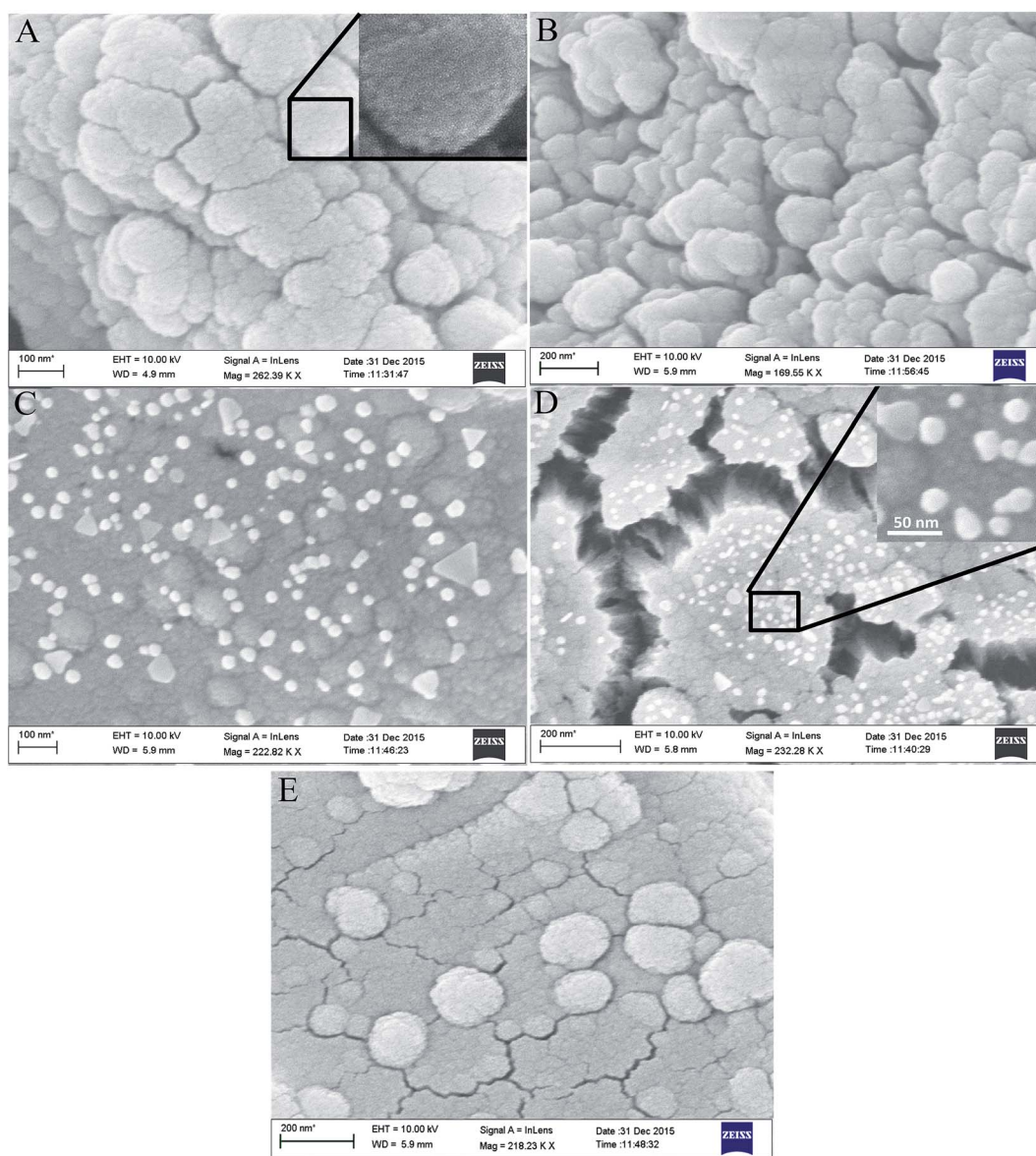


Fig. 2 Scanning electron microscope images of the nanocomposite membranes differing in the amount of added IL as (A) M-1; (B) M-2; (C) M-3; (D) M-4; and (E) M-5. Inset in (A) shows the porous nature of the membrane whereas in the inset of (D) the presence of nanoparticles is shown up.



the surface of M-3 and M-4 only, as can be seen from inset of Fig. 2C and D, respectively. The appearance of these particles at surface indicates the nano-phase separation in the membranes. Further, the appearance of crystallinity in M-3 and M-4 as indicated by XRD measurements (Fig. 1) is attributed to the presence of these nanoparticles.

### 3.3. Transmission electron microscopy

Fig. 3A–E shows the transmission electron microscopic (TEM) images of the prepared nano-composite membranes. As can be seen from Fig. 3A–E, all the membranes seem to be porous in nature, where network like structures appear. A careful examination of Fig. 3A and B reveals that the nano-composite membranes are composed of interconnecting network of near spherical to partially elongated nanoparticles of dimension  $\approx$  40–50 nm, making a mesh like structure. On the other hand, the nano-composite membranes prepared by doping of high IL content *i.e.* M-3 to M-5 are observed to be composed of relatively elongated rod like particles interconnected with each other. Inset of Fig. 3B–E confirms the presence of these elongated structures.

The selected area electron diffraction (SAED) pattern of the prepared membranes is shown in inset of their respective TEM images (Fig. 3A–E). The SAED pattern shows the presence of two bright rings that is in line with two broad peaks observed from XRD studies in case of M-1 to M-5. Further the brightness of the diffraction rings increases while going from M-1 to M-3,

whereas it relatively decreases in case of M-4 and M-5. This observation supports the enhancement in crystallinity of the nano-composite membrane with increase in content of IL till M-3, after which, the crystallinity again decreases. The contradiction between the observance of a large number of diffraction peaks from XRD measurements and only two diffraction rings from SAED pattern, especially in case of M-3, appears to be due to presence of near spherical to hexagonal nano-particles as also observed from SEM measurements (Fig. 2C and D). These nanoparticles are expected to be highly crystalline, giving rise to a large number of diffraction peaks in XRD pattern. We observed these nanoparticles (Fig. 3F) and found them to be highly crystalline as indicated by their diffraction pattern. The appearance of crystallinity in the membranes at particular IL concentrations (M-3 and M-4) can be attributed to the dominating hydrophobic interactions between the alkyl chain of the IL surfactant and hydrophobic chain of the binder along with the electrostatic interactions between the IL head group and the ion exchanger. This expectedly leads to an ordered arrangement of these three components in the membrane. The imbalance of this set of interactions at a very low or higher content of IL disturbs such ordering. At lower concentration of IL, the prevailing interactions seem to be weak due to low number density of IL, whereas at higher concentration, there could be enhanced hydrophobic interactions between alkyl chains of IL itself. This whole process regarding creation of homogeneous crystalline nano domains in the heterogeneous membranes is proposed in Scheme 2.

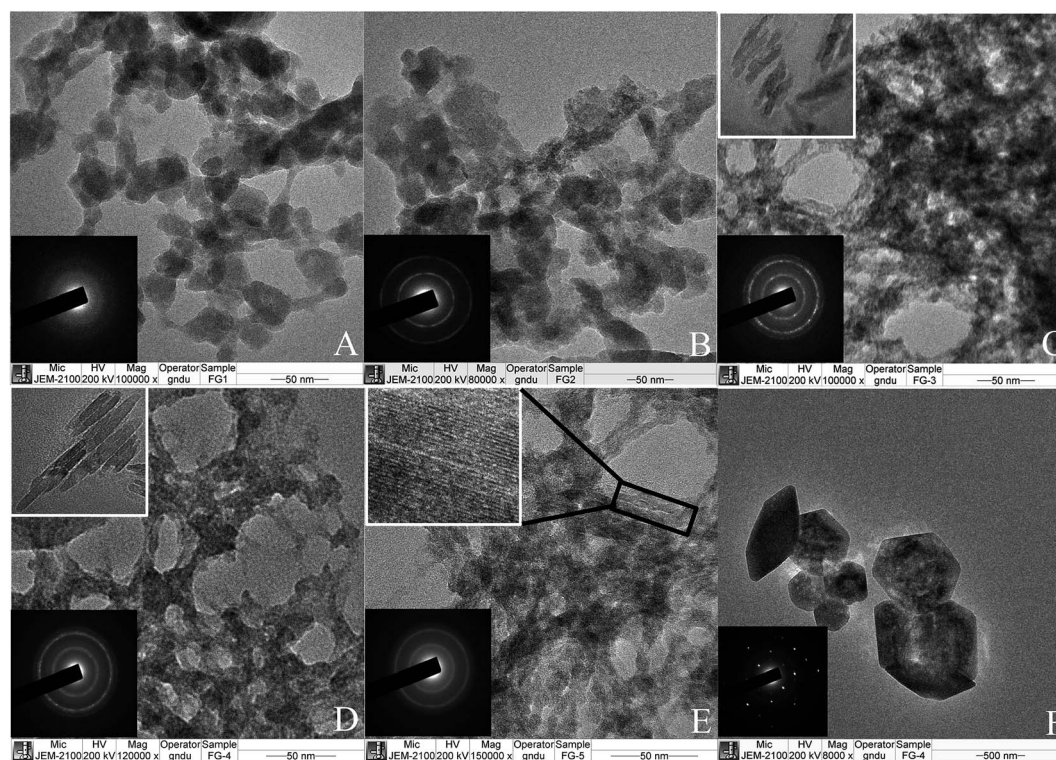
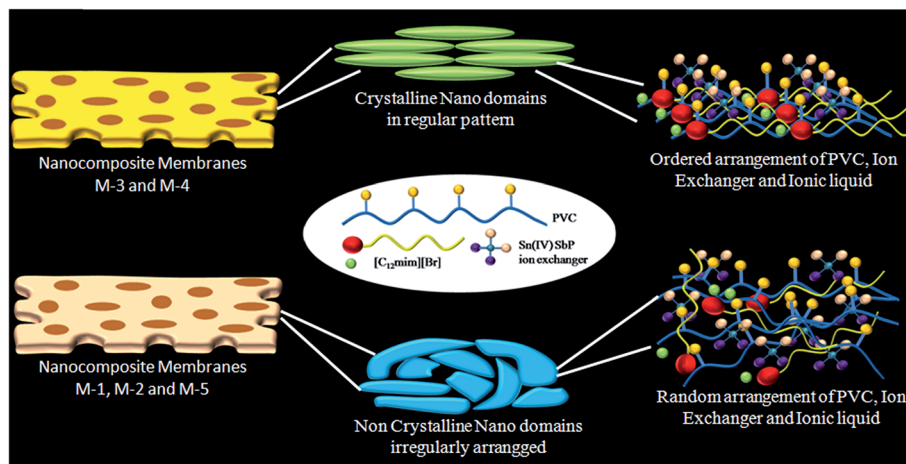


Fig. 3 Transmission electron microscope images of the nanocomposite membranes as (A) M-1; (B) M-2; (C) M-3; (D) M-4; and (E) M-5. Selected area electron diffraction (SAED) pattern for all the membranes is shown in the inset at the bottom of every image. High resolution images showing the crystalline areas in the membrane are shown in the inset of (C–E). TEM image of nanoparticles and SAED pattern for them is shown in the inset of (F).





Scheme 2 The possible mechanism for the crystalline nature of the membranes M-3 and M-4 in comparison to the membranes M-1, M-2, and M-5.

### 3.4. Water content and porosity of the membranes

The data describing the composition and effect of loading of different amount of IL, 1-dodecyl-3-methylimidazolium bromide,  $[C_{12}mim][Br]$ , on key physico-chemical properties such as thickness, water content, IEC (for  $Na^+$ ) and porosity of the prepared membranes *i.e.* M-1 to M-5 is shown in Table 1. As can be seen from Table 1, the thickness of the membranes does not change with varying IL content, which indicates the uniform distribution of IL into the membrane. Interestingly, the water content decreases from 18.2% to 10.0%, while going from M-1 to M-5. The porosity of the prepared membranes has been found to increase with increase in content of IL as also revealed by SEM investigations. The enhanced interactions between alkyl chains of IL, similar to that in a micelle forming large aggregated structures, could lead to increase in porosity. Such increase in porosity provides more space for water molecules to escape and thus is supposed to decrease the water content of the membrane with increase in content of IL. On the other hand, the increasing amount of IL,  $[C_{12}mim][Br]$  having a long hydrophobic alkyl chain could lead to increased interactions between hydrophobic alkyl chain and hydrophobic back bone of PVC, driving out the water of hydration.

### 3.5. Ion exchange capacity

The behavior of prepared membranes is closely related to their structure, especially the spatial distribution of the ionic sites. In heterogeneous ion exchange membranes, ion exchange capacity mainly depends on the content of ion exchanger. With the increase in the content of IL in the membranes, the ion exchange capacity of the fabricated membranes decreases from 1.15 to 0.72 ( $meq\ g^{-1}$ ) as shown in Table 1. The decrease in ion exchange capacity with the increased loading of IL may be attributed to the increased interactions between imidazolium cation of IL with the negatively charged group of ion exchanger. These interactions between IL and ion exchanger seems to be stronger as compared to that between ion exchanger and incoming  $Na^+$ . Thus,  $Na^+$  remains inaccessible to ion exchanger.

With more loading of IL in the matrix, the availability of functional groups in the exchanger decreases further, and this causes the ion exchange capacity to decrease with increase in loading of IL, which is also supported by the decrease in water content of the membranes with increased loading of the IL. It is assumed that the  $[C_{12}mim]^+$  of IL remains in an ordered arrangement, which could align PVC and the exchanger with them leading to enhancement in crystallinity with increasing content of IL.

### 3.6. Electrochemical characterization

The electrochemical characterization of the synthesized membranes was carried out in monovalent ( $NaCl$ ) and bivalent ( $BaCl_2$ ) ionic solutions. Membrane potential and transport number of  $Na^+$  and  $Ca^{2+}$  has been measured and their variation with concentration of electrolyte is provided in Fig. 4(a and b) and 5(a and b), respectively. Membrane potential (Fig. 4) and transport number (Fig. 5) values at different concentrations of both the electrolytes have been found to be highest in case of membrane M-3 as compared to other membranes. This may be due to higher crystallinity of M-3 as compared to other membranes, which provides suitable ionic pathways for the movement of ions.

It is important to mention that both membrane potential and transport number of  $Na^+$  as compared to that of  $Ba^{2+}$  in different membranes under investigation follow the order: M-3 > M-4 > M-5 > M-2 > M-1. The membrane potential and transport number (mobility) of both the electrolytes in the membrane phase increase with increase in concentration of the electrolytes in all the membranes with the exception of M-1 and M-2. The trend of increase in membrane potential and transport numbers with increase in concentration of the electrolytes is due to increase in the number of cations (counter ions) available for transport with increasing concentration. Further, both the membrane potential and transport number have been found to be higher for  $Na^+$  as compared to that of  $Ba^{2+}$ . The lower electrochemical values of different parameters for



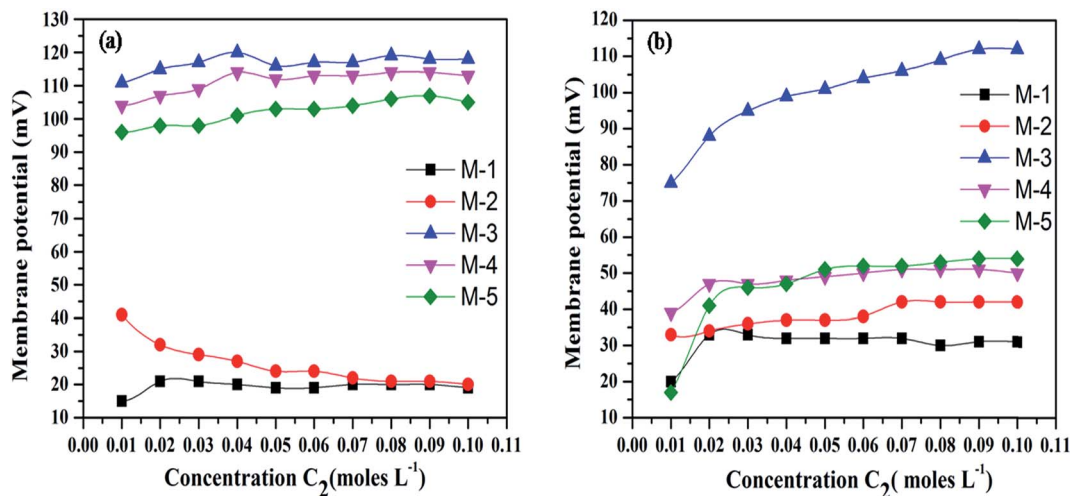


Fig. 4 Effect of concentration on membrane potential values for (a) alkali ( $\text{Na}^+$ ) and (b) alkaline earth ( $\text{Ba}^{2+}$ ) metal ions.

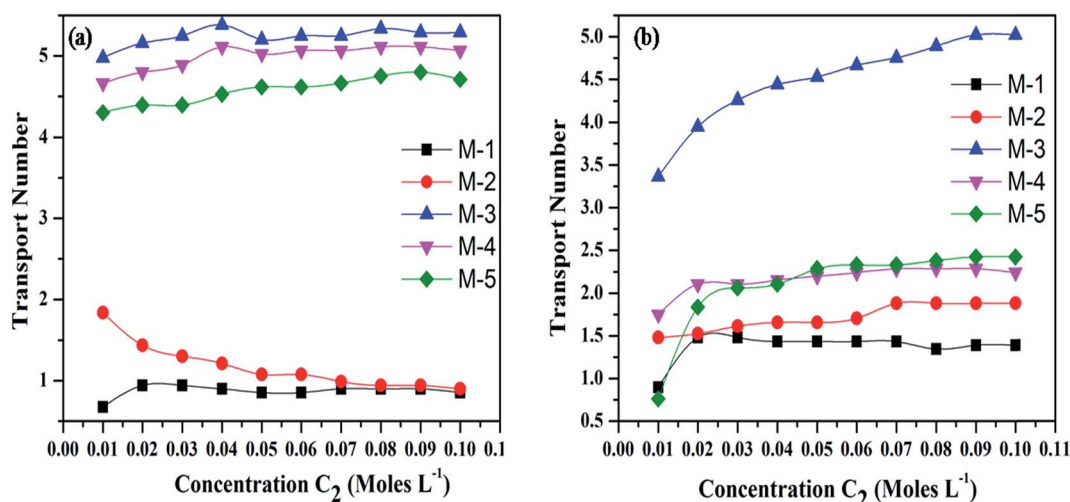


Fig. 5 Effect of concentration on transport numbers for (a) alkali ( $\text{Na}^+$ ) and (b) alkaline earth ( $\text{Ba}^{2+}$ ) metal ions.

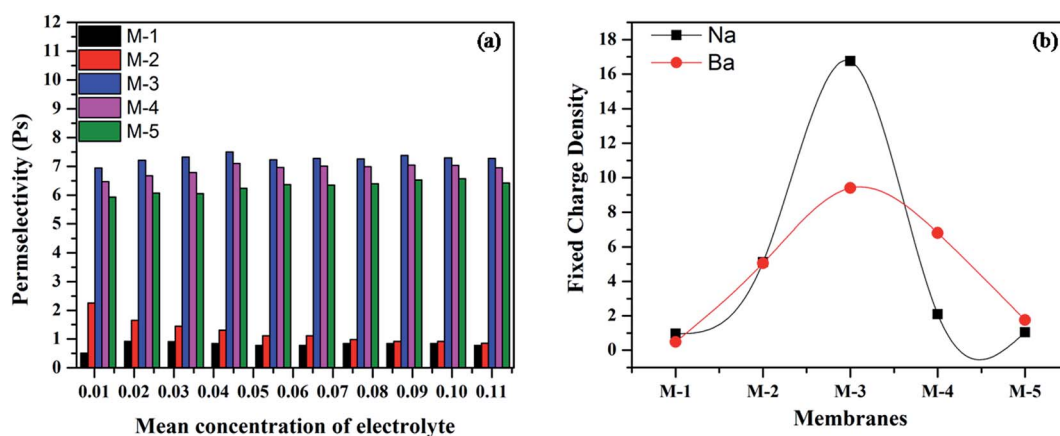


Fig. 6 Variation of permselectivity with mean concentration of (a) alkali metal ions, (b) fixed charge density of different membranes for alkali and alkaline earth metal ions.



bivalent ionic solution in comparison to that of monovalent ions can be explained by the formation of stronger bonds by bivalent ions with the functional groups of the ion exchanger, which leads to decrease in membrane potential, transport number and fixed charge density.<sup>47</sup>

Actually, the electrostatic attraction of bivalent ions with fixed oppositely charged sites prevents the dissociation of cations from the functional groups on the ion exchanger. In addition, larger size of bivalent ions in comparison with that of monovalent ions prevents the penetration of bivalent ions in the pores of ion exchanger, leading to lower values of membrane potential, transport number and fixed charged density.<sup>50,53</sup> Fig. 6a and b show the variation of permselectivity and fixed charge density as a function of concentration for Na<sup>+</sup> and Ba<sup>2+</sup> ions, respectively. Both permselectivity and fixed charge density follow the same trend with respect to variation in composition of membrane as followed by membrane potential and transport number.

Further, the observed values of fixed charge density (Fig. 6b) indicate that larger part of internal fixed charge is inactive. The higher fixed charge density of the membrane for sodium ions is attributed to its smaller hydrated ionic radius as compared to that of barium ions.

## 4. Conclusion

In the present research work, [C<sub>12</sub>mim][Br]-Sn(IV)SbP-PVC nano-composite cation exchange membranes were prepared by solution casting technique. At a moderate concentration of [C<sub>12</sub>mim][Br], the fabricated membranes show higher crystallinity due to enhancement of packing density and nano-phase separations in the membrane. The nano-composite membranes consist of partially elongated nano particles forming a mesh like structure. IL capable of having hydrophobic as well as electrostatic interactions with the PVC and ion exchanger is responsible for creating crystalline homogeneous nano-domains in the heterogeneous membranes. This is expected to provide thermal and mechanical strength to the membrane as well as conserving the membrane structure and morphology upon water intake.<sup>54</sup> The ion exchange capacity and water content of the membranes decreases with increase in loading of IL due to increased interactions between imidazolium cation of ionic liquid with negatively charged group of ion exchanger up to a moderate (M-3) concentration of IL, whereas the increased hydrophobicity of membrane at higher IL content leads to such decrease. The values of various electrochemical properties of the membranes were observed to be higher for Na<sup>+</sup> as compared to that of Ba<sup>2+</sup>, due to formation of stronger bonds by bivalents ions with the functional groups of the ion exchanger.

## Acknowledgements

The authors are thankful to CSIR, Govt of India, for financial assistance wide Project Scheme No. 01(2774)/14/EMR-II. We are thankful to UGC, India, for their UGC-CAS program awarded to the Department of Chemistry, Guru Nanak Dev University,

Amritsar. The infrastructure facility utilized for carrying out this work under the UPE grant is highly acknowledged.

## References

- 1 S. M. Hosseini, S. S. Madaeni and A. R. Khodabakhshi, *Sep. Sci. Technol.*, 2010, **45**, 2308–2321.
- 2 S. M. Hosseini, S. S. Madaeni and A. R. Khodabakhshi, *Sep. Sci. Technol.*, 2011, **46**, 794–808.
- 3 S. M. Hosseini, S. S. Madaeni and A. R. Khodabakhshi, *J. Membr. Sci.*, 2010, **362**, 550–559.
- 4 P. V. Vyas, P. Ray, S. K. Adhikary, B. G. Shah and R. Rangarajan, *J. Colloid Interface Sci.*, 2003, **257**, 127–134.
- 5 R. K. Nagarale, G. S. Gohil, V. K. Shahi, G. S. Trivedi and R. Rangarajan, *J. Colloid Interface Sci.*, 2004, **277**, 162–171.
- 6 S. M. Hosseini, S. S. Madaeni and A. R. Khodabakhshi, *J. Membr. Sci.*, 2010, **351**, 178–188.
- 7 E. Volodina, N. Pismenskaya, V. Nikonenko, C. Larchet and G. Pourcelly, *J. Colloid Interface Sci.*, 2005, **285**, 247–258.
- 8 R. K. Nagarale, V. K. Shahi, R. Schubert, R. Rangarajan and R. Mehnert, *J. Colloid Interface Sci.*, 2004, **270**, 446–454.
- 9 G. J. Hwang, H. Ohya and T. Nagai, *J. Membr. Sci.*, 1999, **156**, 61–65.
- 10 M. Y. Kariduraganavar, R. K. Nagarale, A. A. Kittur and S. S. Kulkarni, *Desalination*, 2006, **197**, 225–246.
- 11 C. O. M' Bareck, Q. T. Nguyen, S. Alexandre and I. Zimmerlin, *J. Membr. Sci.*, 2006, **278**, 10–18.
- 12 T. Xu, *J. Membr. Sci.*, 2005, **263**, 1–29.
- 13 A. Elattar, A. Elmidaoui, N. Pismenskaia, C. Gavach and G. Pourcelly, *J. Membr. Sci.*, 1998, **143**, 249–261.
- 14 A. A. Zagorodni, *Ion Exchange Materials Properties and Applications*, Elsevier, 2007.
- 15 R. K. Nagarale, G. S. Gohil and V. K. Shahi, *Adv. Colloid Interface Sci.*, 2006, **119**, 97–130.
- 16 R. W. Baker, *Membrane Technology and Applications*, John Wiley & Sons Ltd., England, 2nd edn, 2005.
- 17 S. D. Kolev, Y. Baba, R. W. Cattrall, T. N. Tasaki, J. M. Perera and G. W. Stevens, *Talanta*, 2009, **78**, 795–799.
- 18 C. V. Gherasim, G. Bourceanu, R. I. Olariu and C. Arsene, *J. Hazard. Mater.*, 2011, **197**, 244–253.
- 19 R. Guell, E. Anticó, S. D. Kolev, J. Benavente, V. Salvadó and C. Fontàs, *J. Membr. Sci.*, 2011, **383**, 88–95.
- 20 O. Kebiche-Senhadjji, S. Bey, G. Clarizia, L. Mansouri and M. Benamor, *Sep. Purif. Technol.*, 2011, **80**, 38–44.
- 21 H. Ohno, *Electrochemical aspects of ionic liquids*, John Wiley & Sons, New Jersey, 2005.
- 22 H. Ohno, M. Yoshizawa and W. Ogihara, *Electrochim. Acta*, 2004, **50**, 255–261.
- 23 T. Welton, *Chem. Rev.*, 1999, **99**, 2071–2083.
- 24 Q. Zhang, S. Zhang and Y. Deng, *Green Chem.*, 2011, **13**, 2619–2637.
- 25 T. Welton, *Chem. Rev.*, 1999, **99**, 2071–2083.
- 26 C. M. S. S. Neves, J. F. O. Granjo, M. G. Freire, Al Robertson, N. M. C. Oliveira and J. A. P. Coutinho, *Green Chem.*, 2011, **13**, 1517–1526.
- 27 H. Passos, A. Luís, J. A. P. Coutinho and M. G. Freire, *Sci. Rep.*, 2015, **6**, 1–7.



- 28 K. L. V. Aken, M. Beidaghi and Y. Gogotsi, *Angew. Chem., Int. Ed.*, 2015, **54**, 4806–4809.
- 29 R. P. Swatloski, S. K. Spear, J. D. Holbrey and R. D. Rogers, *J. Am. Chem. Soc.*, 2002, **124**, 4974–4975.
- 30 T. Singh, T. J. Trivedi and A. Kumar, *Green Chem.*, 2010, **12**, 1029–1035.
- 31 H. Wang, G. Gurau and R. D. Rogers, *Chem. Soc. Rev.*, 2012, **41**, 1519–1537.
- 32 H. L. Nago, K. Lecompte, L. Hargens and A. B. McEwan, *Thermochim. Acta*, 2000, **357**, 97–102.
- 33 M. Armand, F. Endres, D. R. MacFarlane, H. Ohno and B. Scrosati, *Nat. Mater.*, 2009, **8**, 621–629.
- 34 W. A. Henderson and S. Passerini, *Chem. Mater.*, 2004, **16**, 2881–2885.
- 35 A. Fernicola, F. Croce, B. Scrosati, T. Watanabe and H. Ohno, *J. Power Sources*, 2007, **174**, 342–348.
- 36 N. V. Plechkova and K. R. Seddon, *Chem. Soc. Rev.*, 2008, **37**, 123–150.
- 37 O. Green, S. Grubjesic, S. Lee and M. A. Firestone, *Polym. Rev.*, 2009, **49**, 339–360.
- 38 M. Guo, J. Fang, H. Xu, W. Li, X. Lu and C. L. K. Li, *J. Membr. Sci.*, 2010, **15**, 97–104.
- 39 J. L. Wang, L. L. Wang, R. Feng and Y. Zhang, *Solid State Ionics*, 2015, **278**(1), 144–151.
- 40 N. Gizli, S. Cinarl and M. Demircioglu, *Sep. Purif. Technol.*, 2012, **97**, 96–107.
- 41 A. R. Khodabakhshi, S. S. Madaeni and S. M. Hosseini, *Sep. Purif. Technol.*, 2011, **77**, 220–229.
- 42 L. Shi, Y. Wei and L. Zheng, *Chem. Commun.*, 2013, **49**, 11388–11390.
- 43 D. Li, W. B. Krantz, A. R. Greenberg and R. L. Sani, *J. Membr. Sci.*, 2006, **279**, 50–60.
- 44 S. Kaushal, R. Badru, S. Kumar, S. K. Mittal and P. Singh, *RSC Adv.*, 2016, **6**, 3150–3158.
- 45 G. J. Hwang, H. Ohya and T. Nagai, *J. Membr. Sci.*, 1999, **156**, 61–65.
- 46 L. Ansari, M. Rashid, F. Khan and R. Wahab, *Ind. Eng. Chem. Res.*, 2014, **53**, 14897–14903.
- 47 R. K. Nagarale, G. S. Gohil, V. K. Shahi and R. Rangarajan, *Colloids Surf., A*, 2004, **251**, 133–140.
- 48 V. K. Shahi, S. K. Thampy and R. Rangarajan, *J. Membr. Sci.*, 1999, **158**, 77–83.
- 49 A. Elattar, A. Elmidaoui, N. Pismenskaia, G. Gavach and C. Pourcelly, *J. Membr. Sci.*, 1998, **143**, 249–261.
- 50 X. Li, Z. Wang, H. Lu, C. Zhao, H. Na and C. Zhao, *J. Membr. Sci.*, 2005, **254**, 147–155.
- 51 J. Kerres, W. Cui, R. Disson and W. Neubrand, *J. Membr. Sci.*, 1998, **139**, 211–225.
- 52 D. R. Lide, CRC press Taylor & Francis Group, Florida, 2006–2007.
- 53 G. S. Gohil, V. K. Shahi and R. Rangarajan, *J. Membr. Sci.*, 2004, **240**, 211–219.
- 54 S. Miyanishi, T. Fukushima and T. Yamaguchi, *Macromolecules*, 2015, **48**, 2576–2584.

